HHS Public Access

Author manuscript

FASEB J. Author manuscript; available in PMC 2022 March 01.

Published in final edited form as:

FASEB J. 2021 March ; 35(3): e21425. doi:10.1096/fj.202001634R.

Glycolysis is integral to histamine–induced endothelial hyperpermeability

Athanasios Ziogas[1], **Md Sanaullah Sajib**[2], **Jong-Hyung Lim**[3], **Tiago C. Alves**[1], **Anupam Das**[4], **Anke Witt**[1], **Eman Hagag**[1], **Nikolais Androulaki**[1], **Sylvia Grossklaus**[1], **Michael Gerlach**[5], **Thomas Noll**[4], **Tatyana Grinenko**[1], **Peter Mirtschink**[1], **George Hajishengallis**[3], **Triantafyllos Chavakis**[1], **Constantinos M. Mikelis**[2,§,*], **David Sprott**[1,§,*]

[1.]Institute of Clinical Chemistry and Laboratory Medicine, Faculty of Medicine and University Clinic Carl Gustav Carus, TU Dresden, Dresden, Germany

[2.]Department of Pharmaceutical Sciences, School of Pharmacy, Texas Tech University Health Sciences Center, Amarillo, TX, USA.

[3.]University of Pennsylvania, Penn Dental Medicine, Department of Basic and Translational Sciences, Laboratory of Innate Immunity and Inflammation, Philadelphia, PA, USA.

[4.]Department of Physiology, Faculty of Medicine Carl Gustav Carus, TU Dresden, Dresden, Germany.

[5.]Core Facility Cellular Imaging (CFCI), Faculty of Medicine Carl Gustav Carus, TU Dresden, Dresden, Germany.

Abstract

Histamine-induced vascular leakage is a core process of allergic pathologies, including anaphylaxis. Here we show that glycolysis is integral to histamine-induced endothelial barrier disruption and hyperpermeability. Histamine rapidly enhanced glycolysis in endothelial cells via a pathway that involved histamine receptor 1 and phospholipase C beta signaling. Consistently, partial inhibition of glycolysis with 3-(3-pyridinyl)-1-(4-pyridinyl)-2-propen-1-one (3PO) prevented histamine-induced hyperpermeability in human microvascular endothelial cells, by abolishing the histamine-induced actomyosin contraction, focal adherens junction formation and endothelial barrier disruption. Pharmacologic blockade of glycolysis with 3PO in mice reduced histamine-induced vascular hyperpermeability, prevented vascular leakage in passive cutaneous anaphylaxis and protected from systemic anaphylaxis. In conclusion, we elucidated the role of glycolysis in histamine-induced disruption of endothelial barrier integrity. Our data thereby point

[*]Correspondence: David.Sprott@uniklinikum-dresden.de, Constantinos.Mikelis@ttuhsc.edu.

Author Contribution

A. Ziogas designed and performed research, supervised research, analyzed and interpreted data and wrote the manuscript. M. S. Sajib, J. H. Lim, A. Das, A. Witt, E. Hagag, N. Androulaki, S. Grossklaus and T. Grinenko performed research. T. C. Alves and M. Gerlach performed experiments and interpreted data. T. Noll and P. Mirtschink provided analytical tools and helped in research design. G. Hajishengallis interpreted data and edited the paper. T. Chavakis co-designed research and edited the paper. C.M. Mikelis designed and supervised research and edited the paper. D. Sprott designed and performed research, supervised research, analyzed and interpreted data and wrote the manuscript

[§]These authors contributed equally to this work

Conflict of Interest

The authors declare no competing interests.

to endothelial glycolysis as a novel therapeutic target for human pathologies related to excessive vascular leakage, such as systemic anaphylaxis.

INTRODUCTION

The endothelial barrier of blood vessels controls the transport of solutes and plasma proteins between blood and interstitium. Regulated endothelial permeability contributes to tissue homeostasis, whereas increases in vascular permeability are essential for physiological processes including neovascularization and tissue repair (1). Contrastingly, disruption of the endothelial barrier leads to endothelial hyperpermeability, which is a hallmark of pathologies associated with vascular leakage and edema formation, such as pulmonary edema or anaphylactic shock (2–4).

The integrity of the endothelium is mainly regulated by endothelial cell-cell junctions, such as adherens junctions, through a complex system of transmembrane junctional proteins linked to cytoskeletal binding proteins. The endothelial cell-cell adherens junction protein VE-Cadherin plays a key role as a gatekeeper of the endothelial barrier and of vascular integrity (5–7).

Histamine is a major inducer of vascular hyperpermeability and hence, a central component of permeability-related human pathologies, such as allergy and anaphylaxis (8). Histamine is released from preformed stores in mast cells and basophils and leads to a rapid increase in vascular permeability within minutes. Histamine acts through its four G-protein-coupled receptors (GPCRs), histamine receptor 1 to 4 (H_1R to H_4R) (9). In endothelial cells, histamine induces the disruption of the endothelial barrier through the H_1R and two downstream pathways, one involving the Ras homolog gene family, member A (RhoA) and Rho Associated coiled-coil containing protein kinase (ROCK), and the second involving phospholipase C β (PLCβ)-dependent increases in cytoplasmic calcium levels. The two pathways converge to promote regulatory myosin light chain II (MLC2) phosphorylation, which stimulates the contractile activity of the actin cytoskeleton. The tension generated by actomyosin contraction promotes formation of focal adherens junctions (FAJs) and the consequent formation of junctional gaps thereby disrupting the continuity of the endothelial barrier (10, 11).

Endothelial border disruption is conceivably an energy-dependent process and may therefore require adaptation of the cellular energy metabolism. However, potential metabolic alterations in histamine-stimulated endothelial cells have not been defined. Endothelial cells are highly glycolytic and despite having abundant access to oxygen in the bloodstream, they generate the majority of their ATP production from glycolysis (12). On the other hand, endothelial cells have a relatively low mitochondrial activity and do not rely on oxidative phosphorylation (OXPHOS) (13, 14). Accordingly, strategies targeting elevated endothelial glycolysis have gained attention in the context of vascular endothelial dysfunction and related diseases (15).

Here, we showed that endothelial cells rapidly upregulate glycolysis upon histamine treatment and identified this activation event as crucial for the induction of downstream

processes, such as actin cytoskeleton polymerization, FAJs formation and disruption of endothelial cell-cell contacts. Importantly, pharmacological inhibition of 6-phosphofructo-2-kinase/fructose-2,6-biphosphatase 3 (PFKFB3)-mediated glycolytic activation by the small molecule inhibitor 3PO (16, 17) stabilized endothelial junctions, attenuated endothelial reactions to histamine *in vitro* and prevented histamine-mediated vascular leakage and anaphylactic responses *in vivo*. These findings therefore suggest a potential novel therapeutic treatment for life-threatening systemic anaphylaxis.

METHODS

Mice

Animal studies were carried out according to the protocols approved by the Institutional Animal Care and Use Committees of the Texas Tech University Health Sciences Center and the University of Pennsylvania. C57BL/6 mice, purchased from the Jackson or the Charles River Laboratories, were used at the age of 8 weeks or older.

In vivo permeability assay (Miles assay)

Histamine-induced vascular permeability changes were determined using Evans Blue dye (Fisher Scientific), as previously described (18). C57BL/6 mice were injected intraperitoneally (i.p.) with 3-(3-pyridinyl)-1-(4-pyridinyl)-2-propen-1-one (3PO) (0.07 mg/g; R&D Systems) diluted in 100 μl DMSO as previously described (16). Vehicle control-treated mice received equal amounts of DMSO. Two hours after 3PO injection, mice were anaesthetized by i.p. injections of ketamine and xylazine or by isoflurane inhalation and were injected intravenously (i.v.) with sterile Evans Blue dye (100 μl, 1% in normal saline). After 1 min 5, 15 or 50 ng/μl of histamine hydrochloride (Fisher Scientific) diluted in 20 μl PBS were injected into the shaven back skin, whereas an equal amount of PBS was injected as control. Under these conditions, most agents causing vascular permeability promote the extravasation of Evans Blue within 3–5 min, reaching a maximum effect at approximately 10–15 min (19). Mice were euthanized after 10 min and ~1 cm^2 of skin containing the site of injections was excised. The skin punches were incubated in 500 μl formamide (Sigma-Aldrich) at 55°C for 48 h and the Evans Blue content was determined by absorption at 595 nm. Absorption values of Evans Blue extravasation in histamine-injected skin punches were normalized to the values of control-injected (PBS) skin punches in the same mouse.

Passive cutaneous anaphylaxis

Local anaphylactic response was measured as previously described (10, 20). Briefly, 30 ng of anti-Dinitrophenol-IgE (anti-DNP-IgE; Sigma-Aldrich) diluted in 20 μl of sterile 0.9% NaCl were injected into the dorsal skin of the right ear of C57BL/6 mice. The left ear of mice received an equal volume of saline and served as control. Twenty four hours later, the passively immunized mice were challenged by an i.v. injection of 0.5 mg of Dinitrophenol Human Serum Albumin (DNP-HSA; Sigma-Aldrich) together with 0.08 μg/g Evans Blue (Fisher Scientific) in normal saline. Two hours before DNP-HSA challenge, mice were injected i.p. with 3PO (0.07 mg/g; R&D Systems) diluted in 100 μl DMSO, whereas vehicle control-treated mice received an equal amount of DMSO. Mice were euthanized 30 min after the challenge and ear biopsies were collected. Evans Blue dye was extracted in 400 μl

of formamide (Sigma-Aldrich) at 55°C for 24 h and quantified by measuring light absorption at 595 nm. Absorption values of Evans Blue extravasation in anti-DNP-IgE injected ear biopsies were normalized to the values of control injected (saline) ear biopsies in each mouse.

Active systemic anaphylaxis

Active systemic anaphylaxis model was performed as previously described (10, 20). Briefly, C57BL/6 mice were immunized through i.p. injection of 1 mg Bovine Serum Albumin (BSA; Fisher Scientific) and 300 ng Pertussis toxin (PTX; Invitrogen) in normal saline. Fourteen days later, mice were injected i.p. with 0.07 mg/g 3PO (R&D Systems) diluted in 100 μl DMSO, whereas vehicle control-treated mice received an equal amount of DMSO. Two hours later, mice were challenged with i.v. injection of 2 mg BSA. Mouse survival was monitored for 120 min after the challenge.

Primary Cells and treatments

Primary Human Pulmonary Microvascular Endothelial Cells (HPMEC; Promocell), Human Dermal Microvascular Endothelial Cells (HDMEC; Promocell) and Human Retinal Microvascular Endothelial Cells (HRMEC; Cell Systems) were cultured on 0.2% gelatin-coated plates in Endothelial Cell Growth Medium MV (Promocell) at 37°C and 5% CO_2. Human Umbilical Vein Endothelial Cells (HUVEC; Lonza) were cultured on 0.2% gelatin-coated plates in Endothelial Cell Growth Medium-2 (EGM-2; Lonza) at 37°C and 5% CO_2. All endothelial cells were used in low passages (up to the fifth passage). For *in vitro* stimulations of HPMEC, cells were pre-starved and stimulated in Endothelial Cell Basal Medium MV (Promocell) supplemented with 1% FCS (GIBCO), unless otherwise stated. For partial inhibition of glycolysis, particularly of PFKFB3-mediated glycolysis, cells were pretreated with 20 μM 3PO (Tocris) (Schoors et al., 2014). Histamine (Sigma-Aldrich) was freshly dissolved and added to confluent endothelial monolayers at different concentrations.

Extracellular acidification rate measurement

For real-time analysis of the extracellular acidification rate (ECAR) and oxygen consumption rate (OCR), cells were analyzed with a Seahorse XF-96 Extracellular Flux Analyzer (Agilent). Endothelial cells (1.5 or 2.5 × 10^4 cells / well) were plated on gelatin-coated XF-96 cell culture plates (Agilent) and allowed to form monolayers overnight. The cells were incubated for 1h in unbuffered Seahorse XF Base medium (Agilent) supplemented with 1 g/L glucose (Sigma-Aldrich), 2 mM L-glutamine (Invitrogen) and 1 mM sodium pyruvate (Thermo Fisher Scientific), at pH 7.4 under room air at 37°C and the ECAR or OCR measurement was conducted in the same medium for the different time points, as indicated in the figure legends. For cell treatments, medium with or without histamine (1–100 μM) was injected into the cultures or the background wells via the seahorse injection ports; the values of the respective background wells were used for background correction. Where indicated, histamine receptor 1 (H_1R) inhibitor Diphenhydramine hydrochloride (10 μM; Tocris), phospholipase C (PLC) inhibitor U-73122 (5 μM; Cayman Chemical), protein kinase A (PKA) and cyclic AMP (cAMP) inhibitor H-89 dihydrochloride (10 μM; Tocris), Ras homolog gene family, member A (RhoA) Rho Inhibitor I (1 μg/ml; Cytoskeleton), AKT inhibitor MK2206 (2.50 μM; Cayman Chemical)

and glycolysis attenuator 3PO (20 μM, Tocris) were injected into the cell culture microplates 30 min before histamine injection. Cells treated with Rho inhibitor I were additionally preincubated with the inhibitor for 4h before medium exchange. Appropriate vehicle controls (DMSO and H_2O) were used. In the experiments, in which inhibitors were used, HPMEC were treated with 100 μM histamine. ECAR and OCR data were baselined (21–23) and set as 100% for each well at the time point prior to histamine injection, by using the Wave Desktop 2.3 software (Agilent). Area under the Curve analysis of seahorse ECAR data (24, 25) was perfomed with GraphPad Prism 6 (GraphPad Software Inc.) using ECAR values from the first time point after histamine injection and the time points thereafter.

Glucose uptake

Glucose uptake was measured using a cell-based glucose uptake kit (Cayman Chemical) according to manufacturer's instructions. Briefly, HPMEC were seeded in 96-well clear bottom plates, coated with 0.2% gelatin and left overnight to form monolayers. Cells were then washed with glucose-free Agilent Seahorse XF Assay Medium (Agilent) and incubated in the same medium supplemented with 200 μg/ml 2-NBDG (a fluorescently-labeled deoxyglucose analog) in the presence or absence of 100 μM histamine for 30 min. 2-NBDG cellular uptake was measured in a Synergy™ HT multi-detection microplate reader (Biotek Instruments). Glucose uptake in untreated cells was set as 100% in each experiment.

Phosphofructokinase (PFK) activity

PFK (PFK1 and PFK2) enzymatic activity was determined in HPMEC monolayers treated with medium supplemented with or without 100 μM histamine for 5 min by using a PFK Activity Colorimetric Assay Kit (Biovision) and analyzed with a Synergy™ HT multi-detection microplate reader (Biotek Instruments) according to manufacturer's instructions. PFK activity of unstimulated cells was set as 100% in each experiment.

ATP to ADP ratio

ATP to ADP ratio was measured in HPMEC monolayers treated with medium supplemented with or without 100 μM histamine for 2 min, by using an ADP:ATP ratio assay kit (Sigma-Aldrich) and analyzed with a Synergy™ HT multi-detection microplate reader (Biotek Instruments) according to the manufacturer's instructions. ATP:ADP ratio of untreated HPMEC was set as 100% in each experiment.

ATP measurement

HPMEC were pretreated with 20 μM 3PO for 4 h or with 50 mM 2-DG (Sigma-Aldrich) for 30 min; control samples received DMSO. Cells were then stimulated with 100 μM histamine for 2 min. Thereafter, they were lysed and ATP levels were determined with a luminescent ATP Detection Assay Kit (Abcam) according to the manufacturer's instructions using a Synergy™ HT multi-detection microplate reader (Biotek Instruments). Average values of DMSO-treated control samples were set as 1 in each experiment.

Metabolite quantitation

HPMEC monolayers were treated with medium supplemented with or without 100 μM histamine for 30 min, washed with cold PBS and quenched with an ice-cold solution containing 20% methanol, 0.1% formic acid, 10 μM D4-taurine, 3 mM NaF, 1 mM phenylalanine and 100 μM EDTA. Cell extracts were then collected, frozen immediately, lyophilized overnight and resuspended in water before mass spectrometry analysis. Targeted analysis of glycolytic intermediates was performed by mass spectrometry using a ABSCIEX 5500 QTRAP equipped with SelexION for differential mobility separation (DMS) and acquired using multiple reaction monitoring (MRM) in negative mode. Samples were injected onto a Hypercarb column (3 μm particle size, 4.6×100 mm, Thermo Fisher Scientific) at a flow rate of 0.6 mL/min on an ACQUITY UPLC System. Chromatographic separation was achieved with a gradient of ionic strength: mobile phase A contained 3 mM ammonium formate and 20 μL EDTA; mobile phase B consisted of 30 mM ammonium formate, 20 μM of EDTA and 10% acetonitrile (ROTISOLV LC-MS Grade). The gradient had a duration of 10 min with the following profile: 0 min, 100% A; 1 min, 100% A; 8 min, 0% A; 9 min, 100% A; 10 min, 100% A. Samples were ionized by electrospray into the mass spectrometer with the following source parameters: CUR: 20, CAD: 7, IS: −4500, TEM: 550, GS1: 70 and GS2: 60. DMS was used as an additional separation axis (DT: low, MD: 2-propanol, MDC: high, DMO: 3 and DR: off). DMS-related Separation Voltage (SV) and Compensation Voltage (CoV) for each metabolite was optimized before each experiment. Peak identification and chromatographic separation of all metabolites was confirmed with known standards. Table 1 contains the individual MRM transitions (Q1/Q3) and respective retention times. Peaks were integrated with ElMaven v0.6.1 (Elucidata) and concentrations calculated by interpolation from a standard curve of known concentrations and shown as fold change relative to the control (histamine-untreated) group. Each sample was run twice and its values were averaged. Endogenous taurine was used for normalization, i.e. as a surrogate for cell density.

Live cell imaging

For real-time ratiometric monitoring of intracellular ATP:ADP ratios, the fluorescent biosensor PercevalHR (26) was used. FUGW-PercevalHR, a gift from Gary Yellen (Addgene plasmid #49083), was lentivirally produced as described (27). HPMEC were transduced with the lentivirus and three days later treated with medium supplemented with or without 100 μM histamine. Monolayers were imaged with an Olympus IX 83 spinning disc microscope detecting emission at 525 nm while exciting at 405 nm (corresponding to ADP) and 488 nm (corresponding to ATP). Time series were acquired with a 63x objective for 15 min taking a Z-stack (0.7 μm optical slice thickness) every 25 seconds. After the initial 5 min of acquisition, cells received medium with 100 μM histamine or an equal volume of unsupplemented medium as control. To compute images of ATP:ADP ratios, in each pixel intensities acquired at 488 nm excitation (ATP) were divided by values at 405 nm excitation (ADP). Z-stacks were converted to maximum intensity projections using Fiji software (Schindelin et al., 2012). Resulting ratiometric images were displayed as red-to-yellow pseudocolor gradient for enhanced visibility.

Cytosolic calcium measurement

Cytosolic free Ca^{2+} concentration was measured as previously described (28). Briefly, HUVEC were cultured to 80–90% confluence and pretreated with 20 μM 3PO or vehicle (DMSO) in M199 medium without FBS for 3 hours. Cells were then washed once with Hanks' balanced salt solution (HBSS) and incubated with 1 μM of the calcium dye Fura-2 AM in Dulecco's modified phosphate-buffered saline (DPBS) containing 20 μM 3PO or vehicle for 1 hour. Subsequently, cells were washed twice with DPBS and assay buffer (145 mM NaCl, 2.5 mM KCl, 10 mM HEPES, 10 mM Glucose, 1.2 mM $MgCl_2$, 1.5 mM $CaCl_2$) was added. Readings were taken at excitation wavelenghts of 340 nm and 380 nm with emission detection at 510 nm in both cases (using a plate reader (BioTek Synergy^{Mx}) for 8 cycles (~3 min), after which 100 μM histamine in medium or only medium were added and readings of another 18 cycles (~7 min) were acquired. Data are displayed as ratios of 510 nm emissions at 340 nm and 380 nm excitation (340/380).

Measurement of F-actin to G-actin ratio

Cellular F-actin to G-actin ratio was determined as previously described (29). Briefly, HPMEC were grown to confluence on gelatin coated 96-well black-walled, clear-bottom microplates (Thermo Fisher Scientific) and pretreated with 20 μM 3PO or vehicle control (DMSO) for 4 h, followed by addition of 100 μM histamine in medium or only medium for 5 min. After washing with PBS and fixation with 10% formalin in PBS solution, cells were permeabilized with 0.1% Triton X-100, blocked with 1% BSA, 5% goat serum in PBS for 1 h at RT and stained with Alexa Fluor 488 DNase I for monomeric G-actin (Molecular Probes) and Alexa Fluor 568 Phalloidin for polymeric F-actin (Invitrogen) for 30 min at RT. After the cells were washed three times with PBS, quantification of G-actin and F-actin was performed with a SynergyTM HT multi-detection microplate reader (Biotek Instruments). F-actin to G-actin ratio of control DMSO-treated HPMEC was set as 100% in each experiment.

Immunoblot analysis

HPMEC monolayers were pretreated with 20 μM 3PO or vehicle control (DMSO) for 4 h followed by addition of 100 μM histamine or medium for 6 min, washed with ice-cold PBS and lysed in RIPA lysis buffer supplemented with 1 mM sodium orthovanadate, 2 mM phenylmethylsulfonyl fluoride (PMSF) and protein inhibitor cocktail (Santa Cruz Biotechnology). Cell lysates were centrifuged and the total protein concentration was determined with BCA Protein Assay Kit (Thermo Fisher Scientific). Protein extracts were diluted with NuPAGE LDS Sample Buffer (Thermo Fisher Scientific) and NuPAGE Sample Reducing Agent (Thermo Fisher Scientific), separated in NuPAGE 4–12% polyacrylamide gradient Bis-Tris Protein Gels (Invitrogen) and transferred onto nitrocellulose membranes (Amersham Biosciences). Equal loading was verified by Ponceau Red staining. Membranes were blocked with TBS-T buffer containing 5% w/v non-fat dry milk (BD Bioscienses) and incubated overnight with primary antibodies followed by incubation for 1 h with the appropriate HRP-linked secondary antibodies (R&D Systems). The primary antibodies used were against phospho-VE-Cadherin Tyr-685 (CP1981; ECM Biosciences), actin (ab3280; abcam), phospho-Src Tyr-416 (2101; Cell Signalling) and phospho-MLC2 Thr18/Ser19

(3674; Cell signaling). Staining detection was performed using SuperSignal West Pico or Femto Chemiluminescent Substrates (Thermo Fisher Scientific) with a FUSION FX7 Multimaging System (Peqlab) as previously described (30).

Immunofluorescence

Immunostaining of HPMEC monolayers was performed in 8-well glass bottom chamber slides (Ibidi). Glass surfaces were coated through subsequent treatment with poly-D-lysine solution (Thermo Fisher Scientific) for 30 min, 0.5% glutaraldehyde for 15 min at 4°C and 0.25 mg/ml rat tail collagen I solution (Thermo Fisher Scientific) for 10 min, followed by 70% ethanol for 30 min and endothelial cell culture medium (Promocell) for another 30 min. Between the aforementioned treatments, surfaces were washed with PBS. HPMEC were plated at a density of 2.5×10^4 / well and allowed to form confluent monolayers over 2 days. Cells were treated with 20 μM 3PO or vehicle control (DMSO) for 4 h, after which they were stimulated with 20 μM histamine or medium for 4 min. Monolayers were immediately fixed with 10% formalin in PBS solution for 30 min, stained with antibodies against Vinculin (V9131; Sigma-Aldrich) and VE-Cadherin (AF938; R&D systems), followed by staining with Alexa Fluor 488 labeled donkey anti-mouse (A21202; Thermo Fisher Scientific) and Alexa Fluor 647 labeled donkey anti-goat (A21447; Thermo Fisher Scientific) secondary antibodies. Additionally, Alexa Fluor 568 Phalloidin (Invitrogen) and 4′,6-diamidino-2-phenylindole (DAPI; Merck) were used to label F-actin and nuclei, respectively. Percentages of cells forming FAJs were determined as previously described (10). Briefly, in each field of view, cells exhibiting zipper-like structures positive for Vinculin, VE-Cadherin and F-actin were counted and divided by the number of total visible cells. Fluorescence images were acquired in randomly chosen fields of view using either a Zeiss Observer Z.1 wide field microscope or a Leica SP 5 confocal microscope and image analysis was performed with ZEN Imaging Software (Zeiss) and FIJI software. Images were pseudocolored; the display color of the channels was set as to optimize clarity of merged images.

In vitro endothelial permeability assays

Real time-resolved macromolecular permeability was measured across the monolayers of HPMEC on a 0.4 μM polycarbonate filter membrane separating luminal and abluminal compartments and trypan-blue-labeled albumin flux from luminal to abluminal compartment was calculated as previously described (31). Briefly, 2.5 ml and 9.5 ml of HBSS supplemented with 1.3 mM $CaCl_2$, 1.2 mM $MgCl_2$ and 2% FCS were added into the luminal and abluminal compartments, respectively, and 60 μM of trypan blue-labeled albumin was added to the luminal compartment to create a concentration gradient. HPMEC monolayers were treated with 3PO (20 μM) or vehicle control (DMSO) for 4 h, followed by stimulation with or without 1 mM histamine solution. Trypan blue-labeled albumin diffusion across the two compartments was recorded in real time by a spectrophotometer (Specord 10, Zeiss). Trypan blue was measured at 600 nm wavelength and subtraction of a second measurement at 720 nm was done simultaneously. For each well, absorption values at the time point of addition of histamine or control medium were set as 100%.

For fluorescence microscopy-based permeability assessment, an *in vitro* vascular permeability imaging assay was used (EMD Milllipore). HPMEC were seeded on glass surfaces coated with biotinylated-gelatin and grown to confluence. Monolayers were then pre-treated with 20 μM 3PO or vehicle control (DMSO) for 4 h followed by treatment with medium supplemented with FITC-streptavidin in the presence or absence of 100 μM histamine for 5 min. HPMEC monolayers were fixed with 10% formalin in PBS solution, stained with DAPI and fluorescence pictures were acquired on a Zeiss Observer Z.1 wide field microscope with 40x objective. In each image, the percentage of the FITC-streptavidin-positive area (representing areas of leakage) was determined with FIJI software.

Statistical analysis

Mann-Whitney U test was used for comparison of two groups and two-way ANOVA followed by Sidak's post-hoc analysis or one-way ANOVA with Holm-Sidak's multiple-comparisons test was used for comparison of more than two groups. Mantel-Cox test was used in active systemic anaphylaxis assay. A value of $p < 0.05$ was considered to be statistically significant. Statistical analysis was performed using GraphPad Prism 6 (GraphPad Software Inc.)

RESULTS

Histamine triggers rapid activation of glycolysis in endothelial cells

Histamine rapidly induces vascular leakage through actomyosin contractility and endothelial border disruption (10). As the aforementioned processes are energy-demanding and endothelial cells are dependent on glycolysis for their bioenergetic demands (14), we hypothesized that alterations in glycolytic activity may be necessary for the endothelial cells to adapt to the histamine challenge. To this end, we examined real-time changes in glycolysis of human pulmonary microvascular endothelial cells (HPMEC) upon stimulation with histamine, by measuring their extracellular acidification rate (ECAR). Histamine induced a rapid and immediate increase in ECAR in a concentration-dependent manner (Figure 1A). Given the heterogeneity of endothelial cells from different vascular beds, we repeated the experiment with endothelial cells derived from different vascular beds. Similar to the effect observed in HPMEC, histamine rapidly increased ECAR in primary human dermal microvascular endothelial cells (HDMEC) and in umbilical vein (HUVEC) endothelial cells (Figure 1B,C), whereas hardly any ECAR enhancement was detected in human retinal microvascular endothelial cells (HRMEC) (Figure S1). In contrast to ECAR values, oxygen consumption rates (OCR) were largely unaffected by histamine in HPMEC, HDMEC and HUVEC and only a minor increase was detected shortly after histamine treatment (Figure S2).

We further confirmed the immediate increase in glycolytic activity triggered by histamine by detecting enhanced glucose uptake (Figure 1D) and PFK activity (Figure 1E) in histamine-treated HPMEC. Additionally, we performed targeted metabolomic analysis for the glycolytic pathway intermediates in HPMEC treated with or without histamine. We observed that histamine increased the levels of most glycolytic metabolites in HPMEC. Specifically, glucose-6-phosphate (G6P), fructose-6-phosphate (F6P), fructose-1,6-bisphosphate

(F1,6bP), dihydroxyacetone phosphate (DHAP), 3-phosphoglycerate (3PG), phosphoenolpyruvate (PEP), pyruvate and lactate were significantly higher in histamine-stimulated endothelial cells (Figure 1F).

We next tested whether increased glycolysis in histamine-treated endothelial cells could lead to alterations in cellular ATP:ADP ratios. Indeed, histamine stimulation acutely increased the total endothelial ATP to ADP ratio (Figure 2A). Additionally, using the genetically-encoded fluorescent biosensor PercevalHR, we observed that histamine treatment enhanced cellular ATP:ADP ratios in the nucleus and, intriguingly, instantly led to accumulation of ATP:ADP-rich hotspots at endothelial cell borders (Figure 2B). These results collectively show that endothelial cells rapidly boost glycolysis to fulfill their bioenergetic demands in response to histamine.

Histamine induces glycolysis via the H_1R / PLCβ signaling pathway

To elucidate the molecular mechanisms involved in histamine-induced glycolysis, we investigated the involvement of possible signal transduction pathways. First, we tested whether H_1R, which has a central role in histamine-induced endothelial permeability (10), was also involved in histamine-induced glycolysis upregulation. Pharmacological inhibition of H_1R abolished histamine-induced elevations in ECAR (Figure 3A and B), whereas pharmacological inhibition of H_2R, H_3R or H_4R failed to prevent histamine-induced ECAR (data not shown). Moreover, we observed that pharmacological inhibition of PLCβ, that acts downstream of H_1R, reduced the histamine-induced elevation in ECAR (Figure 3A and B). In contrast, activities of AKT, PKA, cAMP and Rho (Figure 3A and B) were all dispensable for histamine-mediated glycolysis activation. These data suggest that histamine-dependent glycolysis induction in endothelial cells specifically requires the H_1R / PLCβ pathway.

Histamine-mediated disruption of endothelial barrier integrity is mediated by enhanced glycolysis

We next examined whether the rapid glycolysis induction by histamine contributed to disruption of the endothelial barrier. To test this hypothesis, we first inhibited endothelial glycolysis with 2-deoxyglucose (2-DG). However, 2-DG treatment disrupted barrier integrity under baseline conditions, indicating that severe blockage of glycolytic flux by 2-DG stressed endothelial cells and negatively affected their viability (data not shown). Therefore, to achieve a milder inhibition of glycolysis, which would also be therapeutically more relevant, we used 3-(3-pyridinyl)-1-(4-pyridinyl)-2-propen-1-one (3PO), a small molecule inhibitor of the glycolysis activator PFKFB3 (14, 16, 17). To test the extent of 3PO-mediated effects on endothelial energy metabolism, we analyzed ATP levels in histamine-stimulated HPMEC that were pre-treated with 3PO, 2-DG or vehicle (DMSO) (Figure S3). As expected, glycolysis blockage with 2-DG caused a pronounced drop in ATP, while partial glycolysis inhibition with 3PO treatment led to a weak decrease in ATP levels. Furthermore, pretreatment of endothelial cells with 3PO moderately reduced ECAR levels, both under baseline and histamine-stimulated conditions (Figure S4). At the same time, 3PO did not affect H_1R protein levels (data not shown) and it had no influence on downstream signalling, as judged by unaltered histamine-induced cytosolic Ca^{2+} levels of 3PO-treated endothelial cells (Figure S5).

Next, we tested whether mild glycolysis reduction through 3PO treatment affected permeability-related effects of histamine. Endothelial barrier disruption by histamine is linked to actomyosin-driven contractility and rearrangement of cortical actin into radial actin stress fibers anchored to adherens junctions (10). Attenuation of glycolytic activity with 3PO prevented histamine-induced formation of actin stress fibers and disruption of adherens junctions in endothelial cell monolayers, as assessed by VE-cadherin and F-actin staining (Figure 4A). Additionally, 3PO pretreatment of HPMEC blunted the histamine-induced increase in the F-actin to G-actin ratio (Figure 4B) and in MLC phosphorylation (Figure 4C).

The increase in endothelial permeability requires weakening of the adhesive function of VE-Cadherin. Specifically, phosphorylation of VE-cadherin at Tyr685 is involved in endothelial barrier disruption (32). Histamine-mediated phosphorylation of VE-cadherin at Tyr685 as well as phosphorylation of the upstream permeability-promoting Tyrosine-Protein Kinase SRC-1 (Src) (33) in HPMEC were both inhibited by 3PO-treatment (Figure 4C). On the contrary, histamine-induced ERK 1/2 phosphorylation was unaffected by 3PO pretreatment (data not shown), indicating that 3PO does not influence permeability-unrelated histamine receptor signaling. These results suggest that mild inhibition of glycolysis in endothelial cells suppresses histamine-induced cytoskeleton changes and endothelial junction opening.

The tension generated by actomyosin contraction promotes the relocalization of VE-cadherin adhesion complexes to zipper-like structures (designated FAJs), which are characterized by the presence of vinculin and associated F-actin stress fibers (34). Accordingly, attenuation of endothelial glycolysis with 3PO prevented the histamine-induced formation of FAJs at endothelial cell-cell contacts (Figure 4D–E). Together, inhibition of glycolysis with 3PO counteracts the effect of histamine on diminishing endothelial barrier integrity.

Glycolysis inhibition prevents histamine-induced vascular hyperpermeability in vivo and anaphylactic shock

We next investigated the role of glycolysis in endothelial hyperpermeability induced by histamine *in vitro*. Histamine-induced hyperpermeability was abrogated almost completely in 3PO-treated HPMEC monolayers, as assessed by trypan blue-labeled albumin (Figure 5A) and FITC-labeled streptavidin leakage (Figure 5B).

To determine the physiological relevance of our *in vitro* findings, we next examined whether 3PO treatment could prevent histamine-induced vascular hyperpermeability *in vivo*. Strikingly, mice pretreated with 3PO displayed markedly attenuated histamine-induced vascular leakage in two independent models: (i) in the Miles assay, where Evans blue tissue extravasation was triggered directly by local histamine administration (Figure 6A) and (ii) in a passive cutaneous anaphylaxis model, in which Evans blue tissue extravasation was triggered by local mast cell degranulation following antigen exposure in mice pre-treated with respective anti-hapten-specific IgEs (Figure 6B).

To further strengthen our aforementioned *in vivo* data, we examined the effect of 3PO treatment in a mouse model of active systemic anaphylaxis, in which mice were first

sensitized to BSA and then systemically challenged with BSA. Consistent with our findings that glycolysis regulates histamine-induced vascular leakage (Figure 6A–B), pretreatment with 3PO protected mice from anaphylactic shock caused by injection of the allergen and from associated lethality (Figure 6C). These data suggest a profound effect of mild glycolysis inhibition in preventing vascular leakage and related pathologies *in vivo*.

Discussion

Our present findings demonstrate that glycolysis activation is an integral component of histamine-induced endothelial hyperpermeability, which is a key pathomechanistic element of anaphylactic reactions. Endothelial barrier disruption by histamine requires the immediate adaptation of energy supply and endothelial cells engage preferentially in glycolysis rather than oxidative phosphorylation (35). The dependency of histamine-induced endothelial hyperpermeability on glycolysis can be likely attributed to the enhanced and immediate demand for local energy and metabolite production required for reorganization of cell-cell junctional connections and actomyosin contractility. Cellular compartmentalization of multienzymatic glycolytic complexes to specific cellular structures has been previously reported in different cells and can promote local ATP generation and other cellular functions (14, 35, 36).

The importance of enhanced endothelial glycolysis was demonstrated also in other scenarios, where endothelial cells switch from quiescence to an active state. For example, in angiogenesis the glycolytic enzymes PFKFB3 and pyruvate kinase 2 (PKM2) were found to be crucial for migration and proliferation of endothelial cells (12, 37, 38). Furthermore, partial inhibition of glycolysis with 3PO suppressed pathological angiogenesis and led to tumor vessel normalization (39). Additionally, PFKFB3-mediated endothelial glycolysis promotes endothelial inflammation and leukocyte recruitment in the models of pulmonary hypertension and acute lung injury and 3PO treatment alleviated lung edema and protected mice from LPS-induced acute lung injury (40, 41).

We observed that, unlike other endothelial cell types tested here, retinal endothelial cells did not display enhanced glycolysis in response to histamine. It seems plausible that these cells are protected from the effects of histamine, as they contribute to formation of the blood-retina-barrier and therefore may form tighter and less responsive monolayers than endothelial cells from other vascular beds (42). In fact, a previous study demonstrated that H_1R signaling was protective for vascular integrity of brain endothelial cells, to which retinal endothelial cells are related (43). Moreover, considering the role of histamine as a neurotransmitter (44), it seems reasonable that brain and retinal endothelial cells should be able to maintain their vascular integrity in the presence of histamine. Other reports have noted that HRMEC do increase permeability similarly to other endothelial cell types in response to some factors, such as VEGF, but are unresponsive to others, such as IL-6 (45–47). Hence, the distinct responses to histamine of HRMEC, compared to endothelial cells from other vascular beds, provides further evidence for the heterogeneity of vascular endothelial cells from different tissues (48).

We found that in several endothelial cell types histamine stimulation causes an acute boost in glycolysis. This was accompanied by enhanced glucose uptake, elevated levels of glycolytic metabolites and enhanced PFK1 activity. These effects could be partially explained through allosteric activation by fructose-2,6-bisphosphate (F2,6P2), the metabolic product of PFKFB3 (39, 49). We demonstrated that glycolysis activation occurs downstream of histamine-induced signaling and is required for endothelial junction disruption. Specifically, histamine directly and rapidly activated glycolysis in endothelial cells via H_1R, the same receptor implicated in endothelial barrier disruption, and the downstream PLCβ pathway. Glycolysis triggered by histamine was in turn required for MLC phosphorylation and related actomyosin contractility, as well as for VE-cadherin Tyr685 phosphorylation and the resulting loss of endothelial barrier integrity.

We further demonstrated that endothelial glycolysis activation is essential for vascular hyperpermeability induction, as mild glycolysis attenuation with 3PO (17) abolished histamine-induced hyperpermeability. These findings are consistent with a previous report, in which 3PO promoted vascular integrity and EC interconnectivity in quiescent and VEGF-treated endothelial cell monolayers via inhibition of VE-Cadherin endocytosis (39). Histamine-induced permeability, in contrast to permeability induced by other factors like VEGF, does not involve VE-cadherin endocytosis for disruption of endothelial barrier continuity but rather the rapid formation of FAJs, in which vinculin associates with VE-Cadherin to control force-dependent remodeling driven by actomyosin contractility (10). Consistently, the histamine-dependent formation of FAJs was also mediated by increased glycolysis, as it was abrogated in 3PO-treated cells.

Importantly and of direct translational relevance, mice pretreated with 3PO were resistant to vascular leakage when challenged directly with histamine or indirectly in the model of passive cutaneous anaphylaxis, in which vascular leakage is caused by mast cell degranulation and secretion of histamine amongst other permeability-increasing factors. Strikingly, mild glycolysis inhibition by 3PO protected mice from systemic anaphylaxis and associated lethality. One percent of anaphylaxis-related hospitalizations have a fatal outcome (50), while the burden of allergic diseases remains substantial (51). In conclusion, our findings not only provided new insights into the molecular mechanisms underlying histamine-induced glycolysis and the downstream disruption of endothelial barrier integrity but are also therapeutically important. Indeed, treatment with 3PO may offer a novel approach to combat pathological conditions associated with vascular leakage elicited by the acute release of histamine.

Supplementary Material

Refer to Web version on PubMed Central for supplementary material.

Acknowledgements

The authors acknowlegde the support of the Core Facility Cellular Imaging (CFCI) at the Medical Faculty Carl Gustav Carus, Technical University Dresden and technical assistance by Bozena Kesic.

This work was supported by grants from, the Deutsche Forschungsgemeinsachaft (TR-SFB 127 to TC), the NIH/NIDCR DE026152 (to GH and TC) and TTUHSC Office of Research (to CMM).

Abbreviations

2-DG	2-deoxyglucose
3PG	3-phosphoglycerate
3PO	3-(3-pyridinyl)-1-(4-pyridinyl)-2-propen-1-one
DHAP	dihydroxyacetone phosphate
DMSO	dimethyl sulfoxide
ECAR	extracellular acidification rate
F1,6bP	fructose-1,6-bisphosphate
F6P	fructose-6-phosphate
FAJs	focal adherens junctions
G6P	glucose-6-phosphate
H_1R - H_4R	histamine receptor 1–4
HDMEC	human dermal microvascular endothelial cells
HPMEC	human pulmonary microvascular endothelial cells
HRMEC	human retinal microvascular endothelial cells
HUVEC	human umbilical vein endothelial cells
MLC2	myosin light chain II
OCR	oxygen consumption rate
PEP	phosphoenolpyruvate
PFK	phosphofructokinase
PFKFB3	6-phosphofructo-2-kinase/fructose-2,6-biphosphatase 3
PKA	protein kinase A
PLCβ	phospholipase C β
RhoA	Ras homolog gene family, member A
ROCK	Rho Associated coiled-coil containing protein kinase

References

1. Nagy JA, Benjamin L, Zeng H, Dvorak AM, and Dvorak HF (2008) Vascular permeability, vascular hyperpermeability and angiogenesis. Angiogenesis 11, 109–119 [PubMed: 18293091]
2. Park-Windhol C, and D'Amore PA (2016) Disorders of Vascular Permeability. Annu Rev Pathol 11, 251–281 [PubMed: 26907525]

3. van Nieuw Amerongen GP, and van Hinsbergh VW (2002) Targets for pharmacological intervention of endothelial hyperpermeability and barrier function. Vascul Pharmacol 39, 257–272 [PubMed: 12747965]

4. De Bisschop MB, and Bellou A (2012) Anaphylaxis. Curr Opin Crit Care 18, 308–317 [PubMed: 22732436]

5. Giannotta M, Trani M, and Dejana E (2013) VE-cadherin and endothelial adherens junctions: active guardians of vascular integrity. Dev Cell 26, 441–454 [PubMed: 24044891]

6. Dejana E, Orsenigo F, and Lampugnani MG (2008) The role of adherens junctions and VE-cadherin in the control of vascular permeability. J Cell Sci 121, 2115–2122 [PubMed: 18565824]

7. Vestweber D, Wessel F, and Nottebaum AF (2014) Similarities and differences in the regulation of leukocyte extravasation and vascular permeability. Semin Immunopathol 36, 177–192 [PubMed: 24638889]

8. White MV (1990) The role of histamine in allergic diseases. J Allergy Clin Immunol 86, 599–605 [PubMed: 1699987]

9. Thurmond RL, Gelfand EW, and Dunford PJ (2008) The role of histamine H1 and H4 receptors in allergic inflammation: the search for new antihistamines. Nat Rev Drug Discov 7, 41–53 [PubMed: 18172439]

10. Mikelis CM, Simaan M, Ando K, Fukuhara S, Sakurai A, Amornphimoltham P, Masedunskas A, Weigert R, Chavakis T, Adams RH, Offermanns S, Mochizuki N, Zheng Y, and Gutkind JS (2015) RhoA and ROCK mediate histamine-induced vascular leakage and anaphylactic shock. Nat Commun 6, 6725 [PubMed: 25857352]

11. Komarova YA, Kruse K, Mehta D, and Malik AB (2017) Protein Interactions at Endothelial Junctions and Signaling Mechanisms Regulating Endothelial Permeability. Circulation research 120, 179–206 [PubMed: 28057793]

12. De Bock K, Georgiadou M, Schoors S, Kuchnio A, Wong BW, Cantelmo AR, Quaegebeur A, Ghesquiere B, Cauwenberghs S, Eelen G, Phng LK, Betz I, Tembuyser B, Brepoels K, Welti J, Geudens I, Segura I, Cruys B, Bifari F, Decimo I, Blanco R, Wyns S, Vangindertael J, Rocha S, Collins RT, Munck S, Daelemans D, Imamura H, Devlieger R, Rider M, Van Veldhoven PP, Schuit F, Bartrons R, Hofkens J, Fraisl P, Telang S, Deberardinis RJ, Schoonjans L, Vinckier S, Chesney J, Gerhardt H, Dewerchin M, and Carmeliet P (2013) Role of PFKFB3-driven glycolysis in vessel sprouting. Cell 154, 651–663 [PubMed: 23911327]

13. Quintero M, Colombo SL, Godfrey A, and Moncada S (2006) Mitochondria as signaling organelles in the vascular endothelium. Proceedings of the National Academy of Sciences of the United States of America 103, 5379–5384 [PubMed: 16565215]

14. Eelen G, de Zeeuw P, Treps L, Harjes U, Wong BW, and Carmeliet P (2018) Endothelial Cell Metabolism. Physiol Rev 98, 3–58 [PubMed: 29167330]

15. Goveia J, Stapor P, and Carmeliet P (2014) Principles of targeting endothelial cell metabolism to treat angiogenesis and endothelial cell dysfunction in disease. EMBO Mol Med 6, 1105–1120 [PubMed: 25063693]

16. Clem B, Telang S, Clem A, Yalcin A, Meier J, Simmons A, Rasku MA, Arumugam S, Dean WL, Eaton J, Lane A, Trent JO, and Chesney J (2008) Small-molecule inhibition of 6-phosphofructo-2-kinase activity suppresses glycolytic flux and tumor growth. Mol Cancer Ther 7, 110–120 [PubMed: 18202014]

17. Schoors S, De Bock K, Cantelmo AR, Georgiadou M, Ghesquiere B, Cauwenberghs S, Kuchnio A, Wong BW, Quaegebeur A, Goveia J, Bifari F, Wang X, Blanco R, Tembuyser B, Cornelissen I, Bouche A, Vinckier S, Diaz-Moralli S, Gerhardt H, Telang S, Cascante M, Chesney J, Dewerchin M, and Carmeliet P (2014) Partial and transient reduction of glycolysis by PFKFB3 blockade reduces pathological angiogenesis. Cell Metab 19, 37–48 [PubMed: 24332967]

18. Gavard J, Patel V, and Gutkind JS (2008) Angiopoietin-1 prevents VEGF-induced endothelial permeability by sequestering Src through mDia. Dev Cell 14, 25–36 [PubMed: 18194650]

19. Miles AA, and Miles EM (1952) Vascular reactions to histamine, histamine-liberator and leukotaxine in the skin of guinea-pigs. J Physiol 118, 228–257 [PubMed: 13000707]

20. Korhonen H, Fisslthaler B, Moers A, Wirth A, Habermehl D, Wieland T, Schutz G, Wettschureck N, Fleming I, and Offermanns S (2009) Anaphylactic shock depends on endothelial Gq/G11. J Exp Med 206, 411–420 [PubMed: 19171764]
21. Everts B, Amiel E, Huang SC, Smith AM, Chang CH, Lam WY, Redmann V, Freitas TC, Blagih J, van der Windt GJ, Artyomov MN, Jones RG, Pearce EL, and Pearce EJ (2014) TLR-driven early glycolytic reprogramming via the kinases TBK1-IKKvarepsilon supports the anabolic demands of dendritic cell activation. Nat Immunol 15, 323–332 [PubMed: 24562310]
22. Buck MD, O'Sullivan D, Klein Geltink RI, Curtis JD, Chang CH, Sanin DE, Qiu J, Kretz O, Braas D, van der Windt GJ, Chen Q, Huang SC, O'Neill CM, Edelson BT, Pearce EJ, Sesaki H, Huber TB, Rambold AS, and Pearce EL (2016) Mitochondrial Dynamics Controls T Cell Fate through Metabolic Programming. Cell 166, 63–76 [PubMed: 27293185]
23. Lamprecht DA, Finin PM, Rahman MA, Cumming BM, Russell SL, Jonnala SR, Adamson JH, and Steyn AJ (2016) Turning the respiratory flexibility of Mycobacterium tuberculosis against itself. Nat Commun 7, 12393 [PubMed: 27506290]
24. Rice CM, Davies LC, Subleski JJ, Maio N, Gonzalez-Cotto M, Andrews C, Patel NL, Palmieri EM, Weiss JM, Lee JM, Annunziata CM, Rouault TA, Durum SK, and McVicar DW (2018) Tumour-elicited neutrophils engage mitochondrial metabolism to circumvent nutrient limitations and maintain immune suppression. Nat Commun 9, 5099 [PubMed: 30504842]
25. Yarbro JR, and Pence BD (2019) Classical monocytes from older adults maintain capacity for metabolic compensation during glucose deprivation and lipopolysaccharide stimulation. Mech Ageing Dev 183, 111146 [PubMed: 31493436]
26. Tantama M, Martinez-Francois JR, Mongeon R, and Yellen G (2013) Imaging energy status in live cells with a fluorescent biosensor of the intracellular ATP-to-ADP ratio. Nat Commun 4, 2550 [PubMed: 24096541]
27. Kuroda H, Kutner RH, Bazan NG, and Reiser J (2009) Simplified lentivirus vector production in protein-free media using polyethylenimine-mediated transfection. J Virol Methods 157, 113–121 [PubMed: 19114057]
28. Ogola B, Zhang Y, Iyer L, and Thekkumkara T (2018) 2-Methoxyestradiol causes matrix metalloproteinase 9-mediated transactivation of epidermal growth factor receptor and angiotensin type 1 receptor downregulation in rat aortic smooth muscle cells. Am J Physiol-Cell Ph 314, C554–C568
29. Orlova VV, Economopoulou M, Lupu F, Santoso S, and Chavakis T (2006) Junctional adhesion molecule-C regulates vascular endothelial permeability by modulating VE-cadherin-mediated cell-cell contacts. J Exp Med 203, 2703–2714 [PubMed: 17116731]
30. Ziogas A, Maekawa T, Wiessner JR, Le TT, Sprott D, Troullinaki M, Neuwirth A, Anastasopoulou V, Grossklaus S, Chung KJ, Sperandio M, Chavakis T, Hajishengallis G, and Alexaki VI (2020) DHEA Inhibits Leukocyte Recruitment through Regulation of the Integrin Antagonist DEL-1. J Immunol
31. Noll T, Wozniak G, McCarson K, Hajimohammad A, Metzner HJ, Inserte J, Kummer W, Hehrlein FW, and Piper HM (1999) Effect of factor XIII on endothelial barrier function. J Exp Med 189, 1373–1382 [PubMed: 10224277]
32. Wessel F, Winderlich M, Holm M, Frye M, Rivera-Galdos R, Vockel M, Linnepe R, Ipe U, Stadtmann A, Zarbock A, Nottebaum AF, and Vestweber D (2014) Leukocyte extravasation and vascular permeability are each controlled in vivo by different tyrosine residues of VE-cadherin. Nat Immunol 15, 223–230 [PubMed: 24487320]
33. Wallez Y, Cand F, Cruzalegui F, Wernstedt C, Souchelnytskyi S, Vilgrain I, and Huber P (2007) Src kinase phosphorylates vascular endothelial-cadherin in response to vascular endothelial growth factor: identification of tyrosine 685 as the unique target site. Oncogene 26, 1067–1077 [PubMed: 16909109]
34. Huveneers S, Oldenburg J, Spanjaard E, van der Krogt G, Grigoriev I, Akhmanova A, Rehmann H, and de Rooij J (2012) Vinculin associates with endothelial VE-cadherin junctions to control force-dependent remodeling. J Cell Biol 196, 641–652 [PubMed: 22391038]
35. De Bock K, Georgiadou M, and Carmeliet P (2013) Role of endothelial cell metabolism in vessel sprouting. Cell Metab 18, 634–647 [PubMed: 23973331]

36. Real-Hohn A, Zancan P, Da Silva D, Martins ER, Salgado LT, Mermelstein CS, Gomes AM, and Sola-Penna M (2010) Filamentous actin and its associated binding proteins are the stimulatory site for 6-phosphofructo-1-kinase association within the membrane of human erythrocytes. Biochimie 92, 538–544 [PubMed: 20144679]
37. Xu Y, An X, Guo X, Habtetsion TG, Wang Y, Xu X, Kandala S, Li Q, Li H, Zhang C, Caldwell RB, Fulton DJ, Su Y, Hoda MN, Zhou G, Wu C, and Huo Y (2014) Endothelial PFKFB3 plays a critical role in angiogenesis. Arterioscler Thromb Vasc Biol 34, 1231–1239 [PubMed: 24700124]
38. Kim B, Jang C, Dharaneeswaran H, Li J, Bhide M, Yang S, Li K, and Arany Z (2018) Endothelial pyruvate kinase M2 maintains vascular integrity. J Clin Invest 128, 4543–4556 [PubMed: 30222136]
39. Cantelmo AR, Conradi LC, Brajic A, Goveia J, Kalucka J, Pircher A, Chaturvedi P, Hol J, Thienpont B, Teuwen LA, Schoors S, Boeckx B, Vriens J, Kuchnio A, Veys K, Cruys B, Finotto L, Treps L, Stav-Noraas TE, Bifari F, Stapor P, Decimo I, Kampen K, De Bock K, Haraldsen G, Schoonjans L, Rabelink T, Eelen G, Ghesquiere B, Rehman J, Lambrechts D, Malik AB, Dewerchin M, and Carmeliet P (2016) Inhibition of the Glycolytic Activator PFKFB3 in Endothelium Induces Tumor Vessel Normalization, Impairs Metastasis, and Improves Chemotherapy. Cancer Cell 30, 968–985 [PubMed: 27866851]
40. Cao Y, Zhang X, Wang L, Yang Q, Ma Q, Xu J, Wang J, Kovacs L, Ayon RJ, Liu Z, Zhang M, Zhou Y, Zeng X, Xu Y, Wang Y, Fulton DJ, Weintraub NL, Lucas R, Dong Z, Yuan JX, Sullivan JC, Meadows L, Barman SA, Wu C, Quan J, Hong M, Su Y, and Huo Y (2019) PFKFB3-mediated endothelial glycolysis promotes pulmonary hypertension. Proceedings of the National Academy of Sciences of the United States of America 116, 13394–13403 [PubMed: 31213542]
41. Wang L, Cao Y, Gorshkov B, Zhou Y, Yang Q, Xu J, Ma Q, Zhang X, Wang J, Mao X, Zeng X, Su Y, Verin AD, Hong M, Liu Z, and Huo Y (2019) Ablation of endothelial Pfkfb3 protects mice from acute lung injury in LPS-induced endotoxemia. Pharmacol Res 146, 104292 [PubMed: 31167111]
42. Diaz-Coranguez M, Ramos C, and Antonetti DA (2017) The inner blood-retinal barrier: Cellular basis and development. Vision research 139, 123–137 [PubMed: 28619516]
43. Lu C, Diehl SA, Noubade R, Ledoux J, Nelson MT, Spach K, Zachary JF, Blankenhorn EP, and Teuscher C (2010) Endothelial histamine H1 receptor signaling reduces blood-brain barrier permeability and susceptibility to autoimmune encephalomyelitis. Proceedings of the National Academy of Sciences of the United States of America 107, 18967–18972 [PubMed: 20956310]
44. Brown RE, Stevens DR, and Haas HL (2001) The physiology of brain histamine. Progress in neurobiology 63, 637–672 [PubMed: 11164999]
45. Maruo N, Morita I, Shirao M, and Murota S (1992) IL-6 increases endothelial permeability in vitro. Endocrinology 131, 710–714 [PubMed: 1639018]
46. Mesquida M, Drawnel F, Lait PJ, Copland DA, Stimpson ML, Llorenc V, Sainz de la Maza M, Adan A, Widmer G, Strassburger P, Fauser S, Dick AD, Lee RWJ, and Molins B (2019) Modelling Macular Edema: The Effect of IL-6 and IL-6R Blockade on Human Blood-Retinal Barrier Integrity In Vitro. Translational vision science & technology 8, 32
47. Tomita Y, Fu Z, Wang Z, Cakir B, Cho SS, Britton W, Sun Y, Hellstrom A, Talukdar S, and Smith LEH (2020) Long-Acting FGF21 Inhibits Retinal Vascular Leakage in In Vivo and In Vitro Models. International journal of molecular sciences 21
48. Aird WC (2007) Phenotypic heterogeneity of the endothelium: II. Representative vascular beds. Circulation research 100, 174–190 [PubMed: 17272819]
49. Okar DA, Wu C, and Lange AJ (2004) Regulation of the regulatory enzyme, 6-phosphofructo-2-kinase/fructose-2,6-bisphosphatase. Advances in enzyme regulation 44, 123–154 [PubMed: 15581487]
50. Turner PJ, Jerschow E, Umasunthar T, Lin R, Campbell DE, and Boyle RJ (2017) Fatal Anaphylaxis: Mortality Rate and Risk Factors. J Allergy Clin Immunol Pract 5, 1169–1178 [PubMed: 28888247]
51. Rautava S, Kalliomaki M, and Isolauri E (2005) New therapeutic strategy for combating the increasing burden of allergic disease: Probiotics-A Nutrition, Allergy, Mucosal Immunology and Intestinal Microbiota (NAMI) Research Group report. J Allergy Clin Immunol 116, 31–37 [PubMed: 15990769]

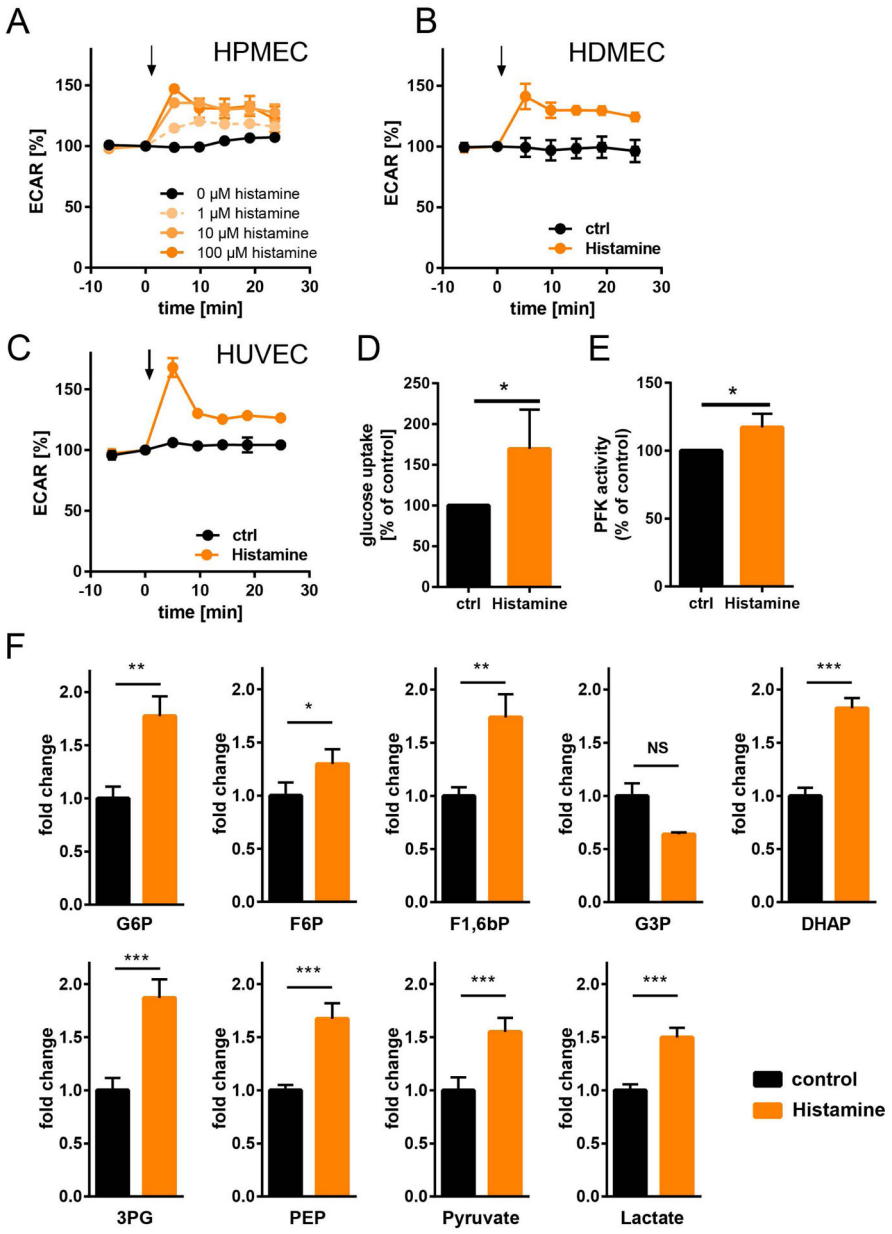

Figure 1: Histamine induces rapid activation of glycolysis in endothelial cells

(A) Real-time changes in extracellular acidification rates (ECAR) of HPMEC treated with the indicated concentrations of histamine or left untreated as control (only medium = 0 µM histamine). Values were baselined and set as 100% for each well at the time point prior to histamine injection (indicated by the arrow) (n=3 different HPMEC donors). (B-C) Real-time changes in ECAR of HDMEC (B) or HUVEC (C) treated with 20 µM histamine or left untreated as control (only medium, control). Values were baselined and set as 100% for each well at the time point prior to histamine injection (indicated by the arrow) (B-C; n=4 experiments). (D) Glucose uptake assessed by 2-NBDG internalisation in HPMEC left unstimulated (control) or treated with histamine for 30 min. Glucose uptake of unstimulated cells was set as 100% in each experiment (n=4). (E) PFK activity in HPMEC left

unstimulated (control) or treated with histamine for 5 min. PFK activity of unstimulated cells was set as 100% in each experiment (n=6). (F) Targeted metabolomic analysis for glycolytic intermediates of HPMEC that were left unstimulated (control) or treated with histamine for 30 min. Data are shown as fold change relative to the control group (n=18 HPMEC cultures; pooled from three independent runs). G6P, glucose-6-phosphate; F6P, fructose-6-phosphate; F1,6bP, fructose-1,6-bisphosphate; G3P, glycerol-3-phosphate; DHAP, dihydroxyacetone phosphate; 3PG, 3-phosphoglycerate; PEP, phosphoenolpyruvate. Data are means ± SEM. *: $p < 0.05$, **: $p < 0.01$, ***: $p < 0.001$ (D-F: Mann-Whitney U test).

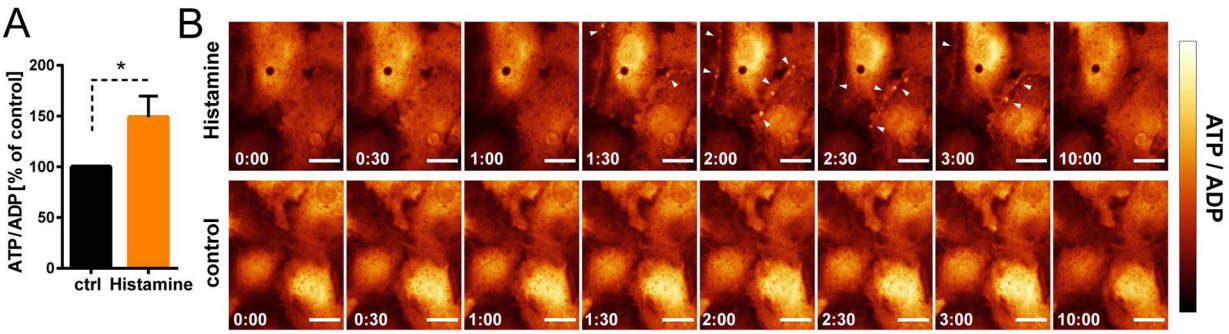

Figure 2: Histamine increases the ATP:ADP ratio in endothelial cells

(A) ATP:ADP ratio in HPMEC left unstimulated (control) or treated with histamine for 2 min. ATP:ADP ratio of unstimulated cells was set as 100% in each experiment (n=4 experiments). Data are means ± SEM. *: $p < 0.05$ (Mann-Whitney U test). (B) Time-resolved imaging of cellular ATP:ADP ratios in HPMEC upon stimulation with histamine or of cells left unstimulated (control). Arrowheads indicate local enhancement of ATP to ADP ratios at cell borders. HPMEC expressing the biosensor PercevalHR were imaged via spinning disc microscopy for 10 min after addition of medium without (control) or with histamine. Exposure wavelengths were set to 405 nm and 488 nm and emission detection was set at 525. Quotients of pixel values acquired at 488 nm and 405 nm excitation were formed to compute pixel values corresponding to ATP:ADP ratios. Grey scales are displayed as red-to-yellow pseudocolor gradient. Displayed images are maximum intensity projections of complete Z-stacks. Scale bars=20 μm. A representative experiment out of three is shown.

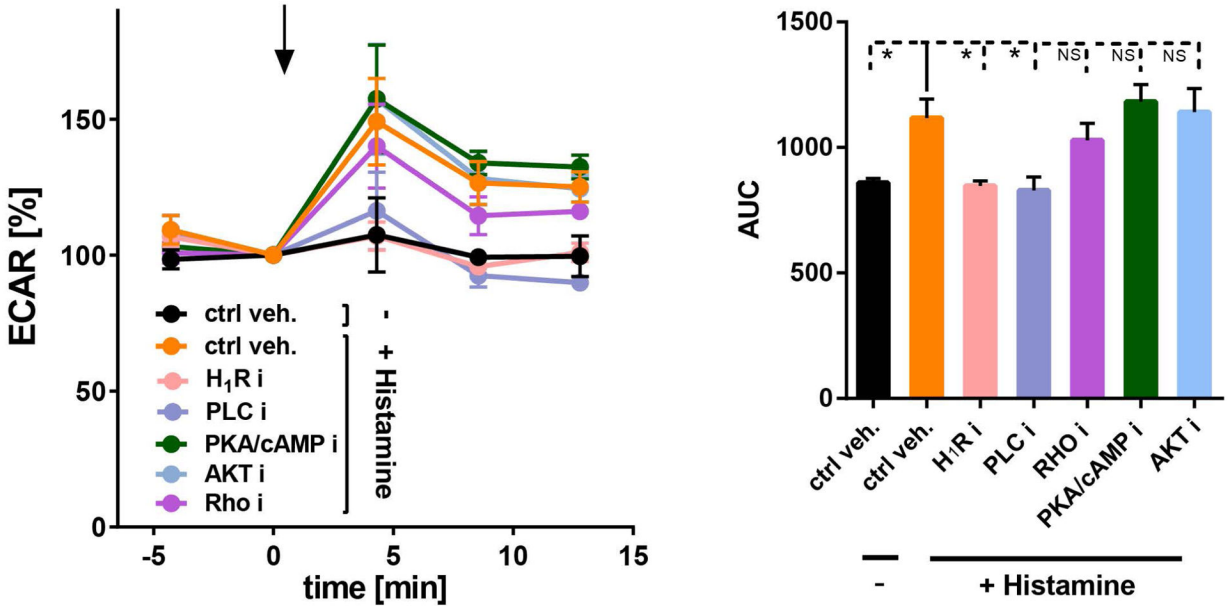

Figure 3: Histamine induces glycolysis via an H_1R / PLCβ signalling pathway

(A) Time-resolved measurement of ECAR changes in HPMEC that were left untreated (only medium with vehicle control) or treated with histamine-containing medium in the presence of vehicle control or pharmacological inhibitors against H_1R, PLCβ, PKA and cAMP, RhoA or AKT. Inhibitors or respective control vehicles were pre-incubated in cultures before histamine or medium treatment, as described in the Methods. Values were baselined and set as 100% for each well at the time point prior to histamine injection (indicated by the arrow). (B) Area under the curve analysis of ECAR changes upon histamine stimulation (AUC analysis was performed for the area between the first and the third ECAR measurement time point after histamine injection). Data are means ± SEM (n=3 experiments). *: $p < 0.05$ (1-way ANOVA with Holm-Sidak's multiple-comparisons test). NS, non-significant.

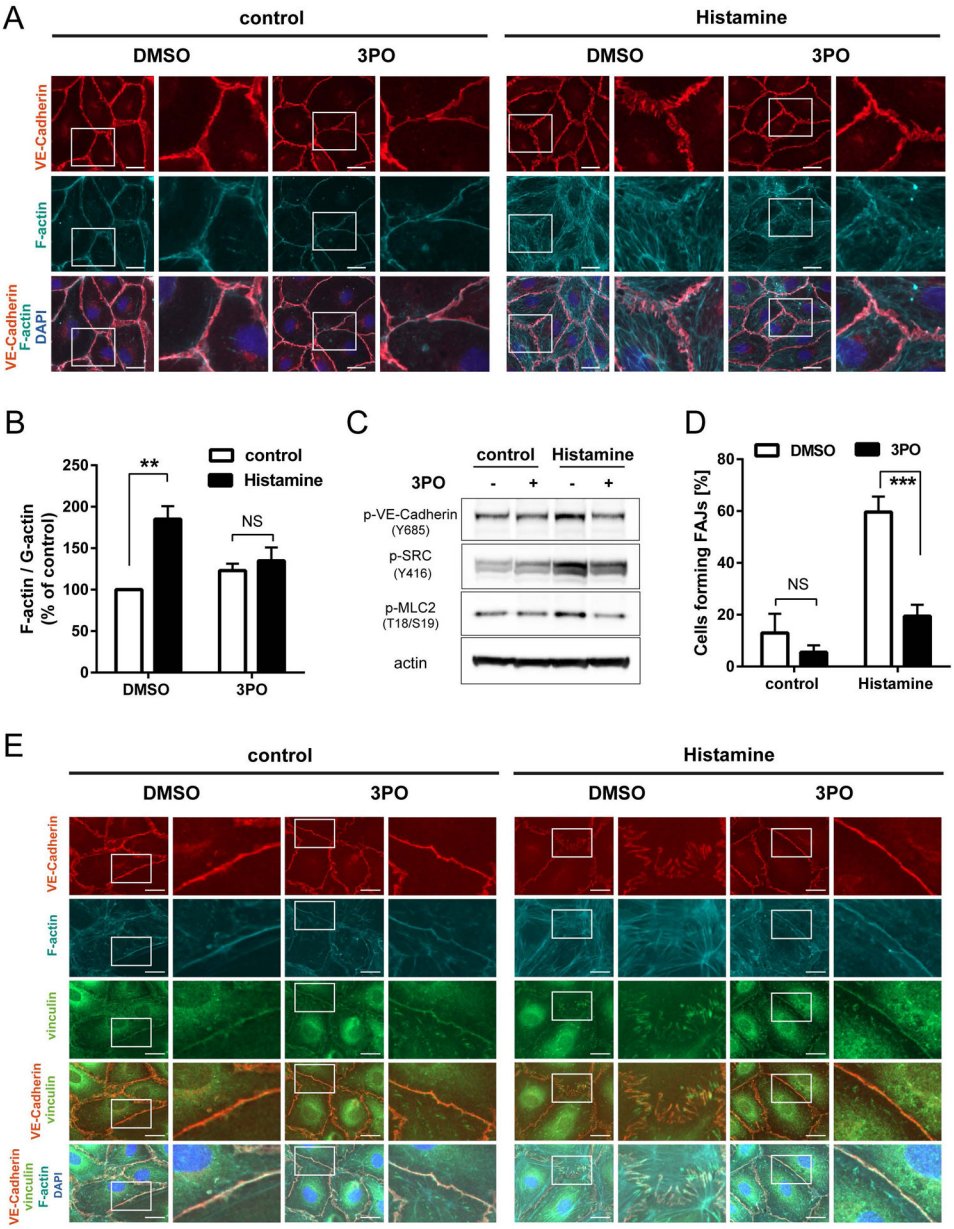

Figure 4: Attenuation of endothelial glycolysis blocks the formation of histamine-induced F-actin stress fibres and FAJs

(A) Representative fluorescence images of HPMEC monolayers that were pretreated with 3PO or vehicle (DMSO) for 4 h followed by addition of histamine or medium (control) for 4 min. Cells were stained for VE-cadherin (red), F-actin (with rhodamine-phalloidin, cyan) and nuclei with DAPI (blue). The areas indicated by the square are displayed in higher magnification on the right side of the original image. Pseudocolored images are shown. Scale bars=20 μm. Representative images from one experiment out of 3 are shown. (B) F-actin to G-actin ratio of HPMEC pretreated with 3PO or vehicle (DMSO) for 4 h followed by addition of histamine or medium (control) for 5 min. F-actin to G-actin ratio of control-treated (DMSO, no histamine) HPMEC was set as 100% in each experiment (n=3). (C) Representative cropped blot images of HPMEC pretreated with 3PO or vehicle (DMSO, -)

for 4 h followed by addition of histamine or medium (control) for 6 min. Cell lysates were immunoblotted for phospho-VE-Cadherin (Y685), phospho-SRC (Y416), phospho-MLC2 (T18/S19) and actin. One experiment representative of 6 experiments is shown. (D-E) HPMEC monolayers were pretreated with 3PO or vehicle DMSO for 4 h and subsequently treated with histamine or medium (control) for 4 min. Cells were fixed and stained for VE-cadherin (red), vinculin (green), F-actin was labelled by rhodamine-phalloidin (cyan) and nuclei were labelled with DAPI (blue). In (D), quantification of the percentage of cells forming focal adherens junctions (FAJs; defined as colocalization of vinculin, F-actin and discontinuous VE-cadherin signal in interendothelial junctions) is shown (n=5 experiments). In (E), representative fluorescence images are depicted. Images are shown in pseudocolor. The areas indicated by the square are shown in higher magnification on the right side of the original image. Scale bars=20 μm. Data are means ± SEM. **: $p < 0.01$, ***: $p < 0.001$ (B, D: 2-way ANOVA with Sidak's multiple-comparisons test). NS, non-significant.

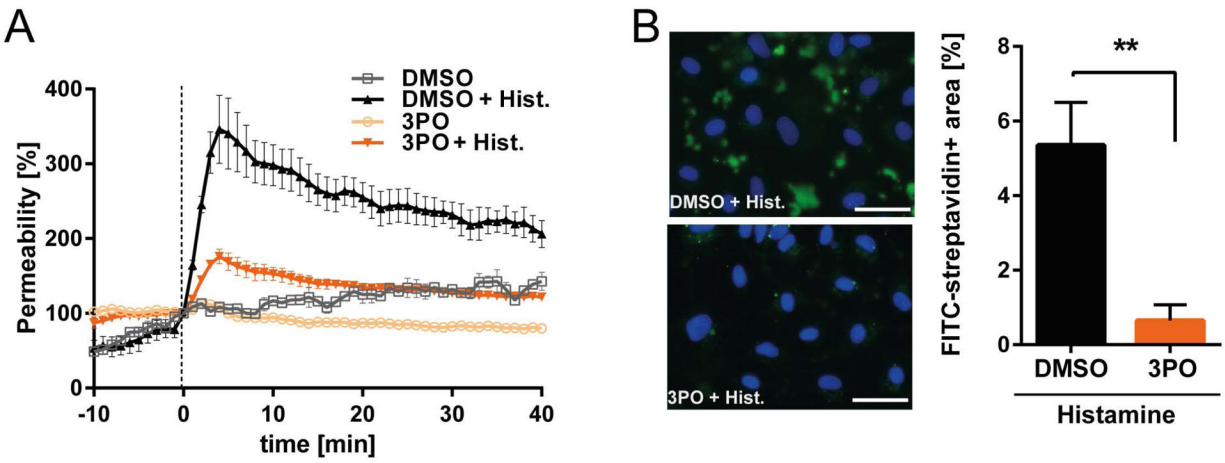

Figure 5: Inhibition of glycolysis reduces histamine-induced endothelial permeability

(A) *In vitro* macromolecular permeability assay in HPMEC monolayers pre-exposed to 3PO or DMSO (control) for 4 h followed by treatment with histamine or medium, as described in the Methods. Increase in permeability and its recovery was recorded in real-time for 40 min. Values at the time point of addition of histamine or medium (indicated by the vertical dotted line) were set as 100% in each well (n=3 experiments). (B) Staining of FITC-streptavidin leakage through histamine-treated endothelial monolayers. HPMEC were pre-treated with 3PO or vehicle (DMSO) for 4 h, after which FITC-streptavidin was added in the presence or absence of histamine for 5 min, as described in the Methods. (left) Representative fluorescence images of FITC-streptavidin leakage (green) through endothelial monolayers are displayed; nuclei are visualized with DAPI staining (blue). (right) Percentage of the FITC-streptavidin-leakage-positive area was quantified in each image (n=6 images per condition; data are from one experiment, representative of three). Data are means ± SEM. **: $p < 0.01$; (B: Mann-Whitney U test).

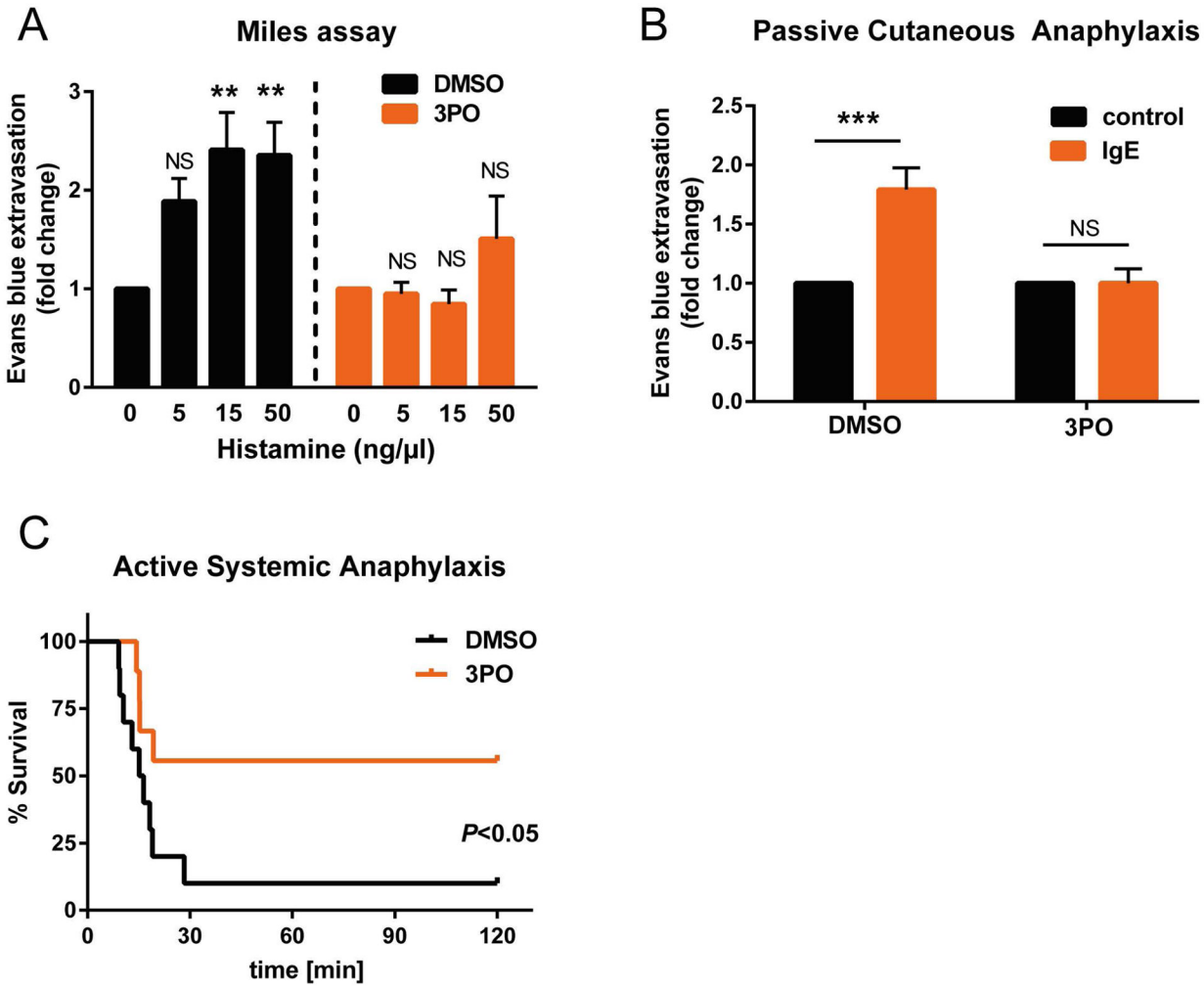

Figure 6: Pharmacological blockade of glycolysis impairs histamine-induced vascular permeability and anaphylactic reaction in vivo

(A) Quantification of histamine-mediated vascular leakage *in vivo* via Miles Assay in vehicle control-treated (DMSO) and 3PO-treated mice. Evans Blue extravasation in skin biopsies was determined after subdermal injection of 0, 5, 15 and 50 ng/µl of histamine diluted in PBS. Mice were injected i.p. with either 3PO or vehicle (DMSO) 2 h prior to histamine application. Data were expressed as the ratio of Evans Blue extravasation promoted by histamine over the Evans Blue extravasation promoted by the control injection (PBS, indicated as 0 ng/ml histamine) in the same mouse. Values of control (0 ng/µl histamine)-treated samples were set as 1 for each mouse (n=4 mice per group). (B) Induction of passive cutaneous anaphylaxis was conducted in mice injected into ear skin with anti-DNP-IgE or with normal saline (control). Twenty four hours later, mice received i.v. injections of DNP-HSA with Evans Blue dye in normal saline to trigger dye leakage. Mice were either treated with DMSO or 3PO by i.p. injections 2 h before injection of DNP-HSA. Data were expressed as the ratio of Evans Blue extravasation promoted by anti-DNP-IgE over Evans Blue extravasation promoted by the control injection (saline) of the same mouse. Values of saline injected (control) ear biopsies were set as 1 for each mouse (n=11 mice per group). (C) Assessment of mouse survival in vehicle control-treated (DMSO) versus 3PO-

treated mice during active systemic anaphylaxis. Mice were sensitized with BSA and PTX and challenged 14 days later with BSA. Mouse survival was monitored for 120 min. 3PO or DMSO treatment took place by i.p. injections 2h before the second BSA challenge (n=9–10 mice per group). Data are means ± SEM. **: $p < 0.01$, ***: $p < 0.001$ (A-B: 2-way ANOVA with Holm-Sidak's multiple-comparisons test; C: Mantel-Cox test). NS, non-significant.

Table 1 -

MRM transitions (Q1/Q3) for each detected metabolite and corresponding retention time.

Metabolite	Q1/Q3	Retention time (min)
Glucose-6-Phosphate	259/97	5.32
Fructose-6-Phosphate	259/97	5.50
Fructose-1,6-bisPhosphate	339/79	6.18
Dihydroxyacetone Phosphate	169/97	4.92
Glycerol-3-Phosphate	171/79	4.71
3-Phosphoglycerate	185/97	5.46
Phosphoenolpyruvate	167/79	5.66
Pyruvate	87/87	5.30
Lactate	89/89	4.00
Taurine	124/80	2.44